EXPERIMENTAL INVESTIGATION ON THE EFFECT OF BAR BUCKLING ON ULTIMATE DRIFT CAPACITY IN REINFORCED CONCRETE BEAMS

Shubham TRIVEDI[1)], Hitoshi SHIOHARA[2)] and Seitaro TAJIRI[3)]

1) Ph.D. Candidate, Department of Architecture, Graduate School of Engineering,
The University of Tokyo, shubham@rcs.arch.t.u-tokyo.ac.jp
2) JAEE Member, Professor, Department of Architecture,
The University of Tokyo, shiohara@arch.t.u-tokyo.ac.jp
3) JAEE Member, Associate Professor, Department of Architecture,
The University of Tokyo, tajiri@arch.t.u-tokyo.ac.jp

ABSTRACT: This report summarizes an experimental investigation of reverse cyclic response of reinforced concrete beams with different longitudinal bar diameter conducted to understand the influence of longitudinal bar-buckling on ultimate drift capacity. Experimental setup and measurement schemes, including digital monitoring of concrete surface deformation for photogrammetric analysis, implemented in this investigation are briefly described. General specimen response and damage progression is comparatively discussed. Measurements obtained from displacement sensors and photogrammetry, expressed in the form of axial strains and lateral bulging deformations around the critical section, are analyzed to understand the progression of strength deterioration at large deformation levels. On the basis of the comparative discussion of the observed response, it is concluded that no significant improvement in drift capacity can be achieved by using large diameter bars.

Key Words: RC beams, Bar buckling, Ultimate drift capacity, Experimental investigation, Photogrammetric analysis

1. INTRODUCTION

Accurate estimation of ultimate drift capacity in reinforced concrete elements has become increasingly important with the advent of performance-based seismic design. One of the commonly reported ultimate state of ductile RC elements is the buckling of longitudinal reinforcing bars[1]. Reinforcing bars subjected to large stress reversals have been identified as particularly susceptible to bar-buckling[2]. Concrete elements designed to preclude all other modes of failure would thus be limited in their capacity of undergo repeated loading cycles by the instability of the longitudinal reinforcement. Provision of adequate stirrups has been understood as one of the primary means to avoid failure through bar-buckling[3].

In this research, influence of bar-buckling on the ultimate drift capacity in reinforced concrete beams is investigated by testing specimens reinforced with differing diameters of longitudinal reinforcing bars. Sturdier bars are expected have greater resistance to buckling and therefore ensure larger lateral deformation capacity. An innovative measuring scheme is implemented using photogrammetry to precisely

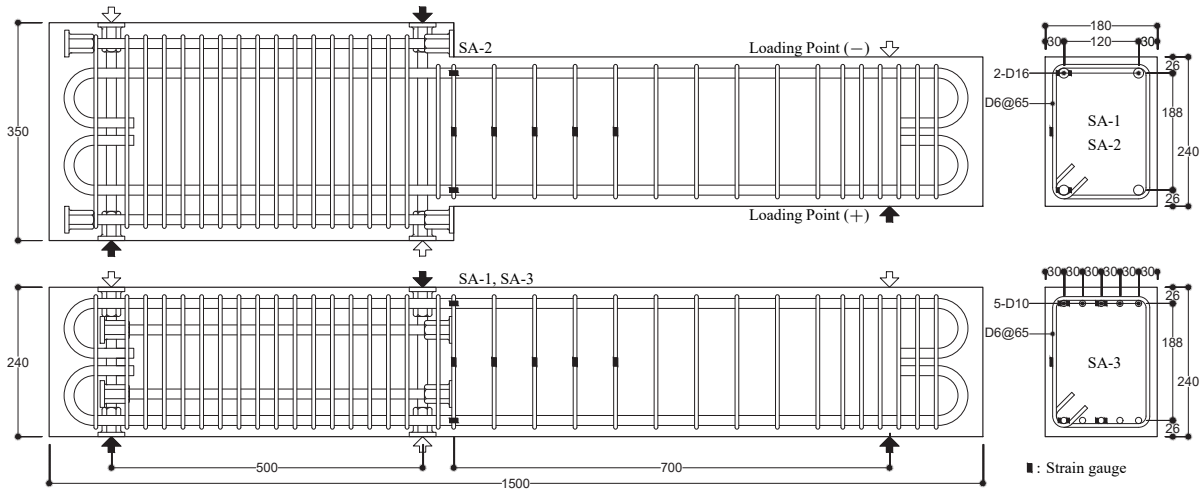

Figure 1: Specimen details (all dimensions are in mm**)**

examine the specimen response. Following sections detail the specimens being investigated and the instrumentation used to study the obtained response. Finally, the obtained response is comparatively discussed.

2. EXPERIMENT SETUP

A total of three specimen were tested in this study. In addition to a specimen (SA-3) with smaller diameter longitudinal reinforcement bars to study the aforementioned effect of bar-buckling, another specimen (SA-2) with conventional stub configuration was also tested to establish equivalence with the proposed testing configuration. Geometry of the specimen and the reinforcing details are illustrated in Figure 1. In the stub-less specimen configuration (SA-1 and SA-3,) the stub portion was reinforced with additional headed bars but a uniform section shape was maintained. Specimen SA-1 and SA-2 were fabricated with identical materials while specimen SA-3 differs only in the longitudinal reinforcement. Material specifications for each specimen are listed in Table 1. Concrete strength is reported as the test value obtained from cylinder compressive tests conducted prior to the loading of each specimen as expressed in Figure 5. It must be noted that different yield strengths were recorded for D-16 and D-10 bars in spite of the same SD345 steel grade.

The specimens were tested in a cantilever configuration using the loading frame shown in Figure 2. A three-point alternate loading was provided using PC rods. The stub portion was supported by a rigid frame while the end of the cantilever portion was connected to the loading arm of the frame. The specimen was thus arranged to exhibit cantilever response in the 700 mm span with the critical section at the edge of the middle loading attachment. Displacement measurements were recorded using laser displacement sensors as illustrated in Figure 3. Displacement at the loading tip and rotation at the end of hinge region were measured using sensors attached to a reference frame fixed close to the critical section on the specimen stub portion. Additionally, photogrammetric measurements were also captured over the grid indicated in Figure 3 by post-processing[4] the photographic data. A monochromatic patterned target was placed at each grid point and phase-only correlation was used to digitally record the position of each target through post-processing.

Applied loading history is illustrated in Figure 4. 2 load controlled cycles were applied prior to the initiation of repetitive deformation controlled cycles. 3 cycles were performed for each target drift and successive target drifts were applied with 1 % increment terminating in 3 cycles at 6 % drift.

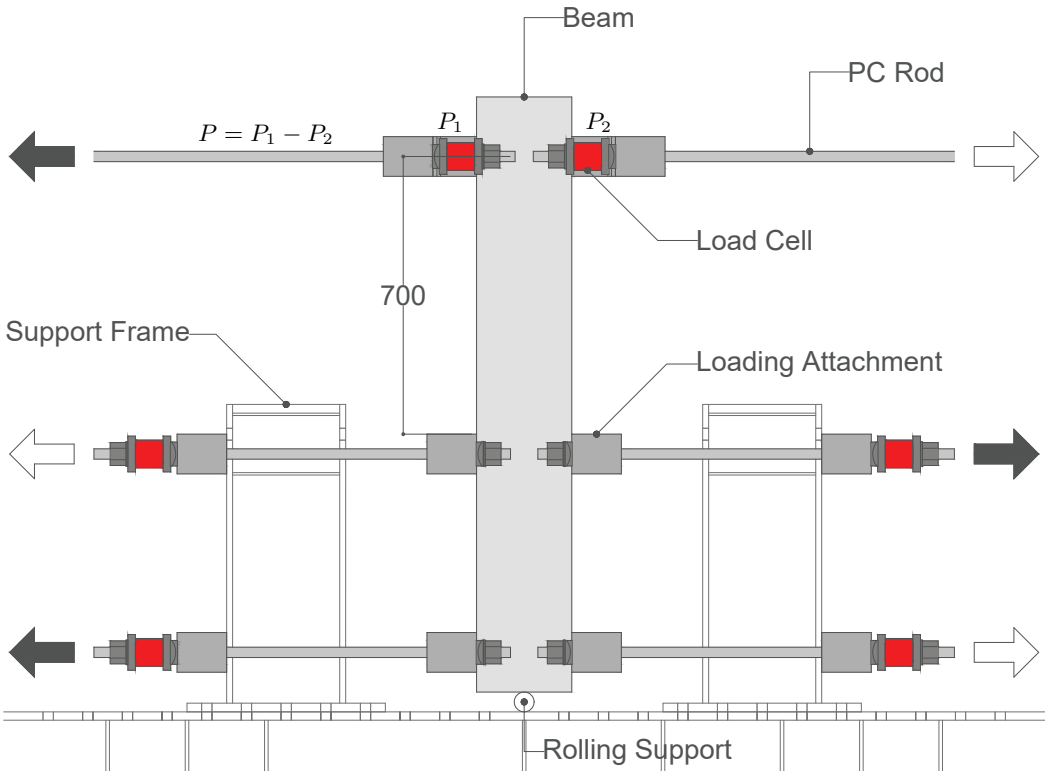

Figure 2: Loading frame (all dimensions are in mm**)**

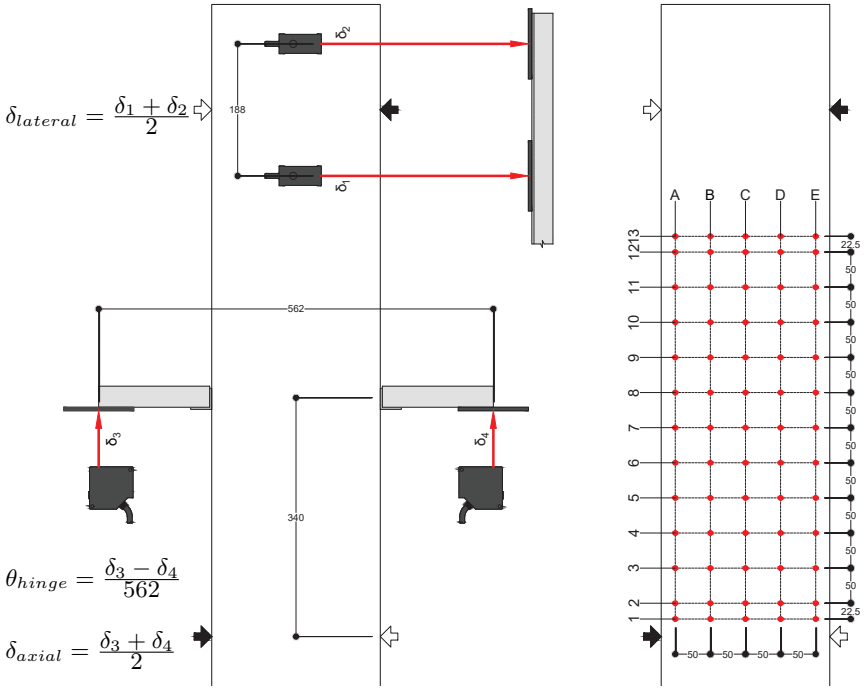

Figure 3: Measuring scheme (all dimensions are in mm**)**

3. OBSERVATIONS

General overview of damage progression in the three specimens throughout the cyclic loading regime is expressed in Figure 6. Each image shows the specimen state at the completion of the indicated loading

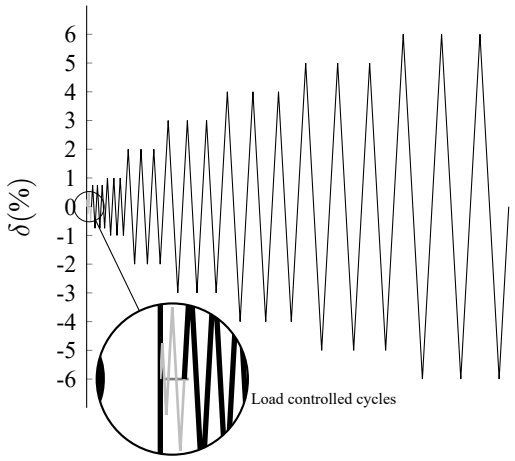

Figure 4: Applied loading history

		SA-1	SA-2	SA-3
f_c'	(MPa)	28.2	29.3	29.6
ρ	(%)	1.04	1.04	1.02
ρ_t	(%)	0.56	0.56	0.58
f_y	(MPa)	395	395	362
f_{yt}	(MPa)	348	348	348

f_c': Concrete compressive strength
ρ: Longitudinal reinforcement ratio
ρ_t: Transverse reinforcement ratio
f_y: Longitudinal reinforcement yield strength
f_{yt}: Transverse reinforcement yield strength

Table 1: Specimen specifications

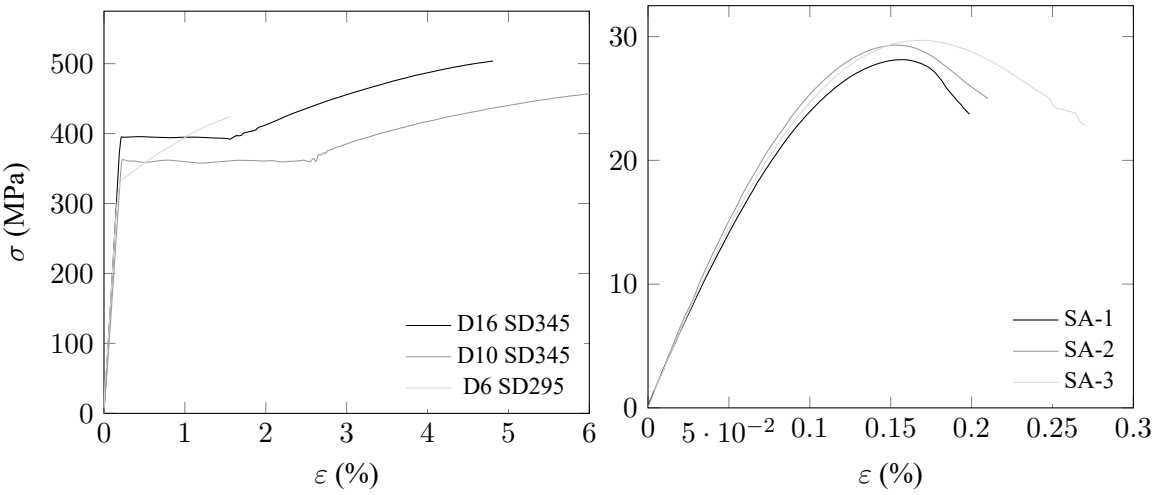

(a) Reinforcing bars **(b) Concrete**

Figure 5: Material characteristics

cycle. All three specimen showed generally similar crack progression starting from small deformation through to large deformation cycles. Diagonal cracks that appeared after the 3 % cycle widened after repeated loading until concrete at the intersection started to spall and lead to loss of strength. Corresponding load deformation behavior of the specimens are compared in Figure 7. Yield (V_y) and ultimate (V_u) strengths calculated as per ACI 318-14 [5] along with the yield point inferred from the strain gauge readings are also indicated for reference. SA-2 exhibited very similar response to SA-1 including the yielding point and the post elastic strength gain due to strain hardening. Ultimately, rapid strength loss was also observed during the 5 % drift cycle in both the specimens. This result validates the reproducibility of expected cantilever response even with the stub-less specimen configuration. SA-3 developed a lower yield and peak strength as compared to SA-1 due to slightly lower yield strength of the D-10 reinforcing bars. Strength loss characteristics of the two specimens were, however, very similar as both specimens sustained loading cycles at 4 % drift before registering significant loss in strength during the 5 % drift cycles.

Displacement data recorded through photogrammetry was utilized to calculate concrete surface deformations in the form of axial and lateral strains. Figure 8 illustrates the progression of axial strain throughout the successive loading cycles at each vertical grid A to E between the critical section and the

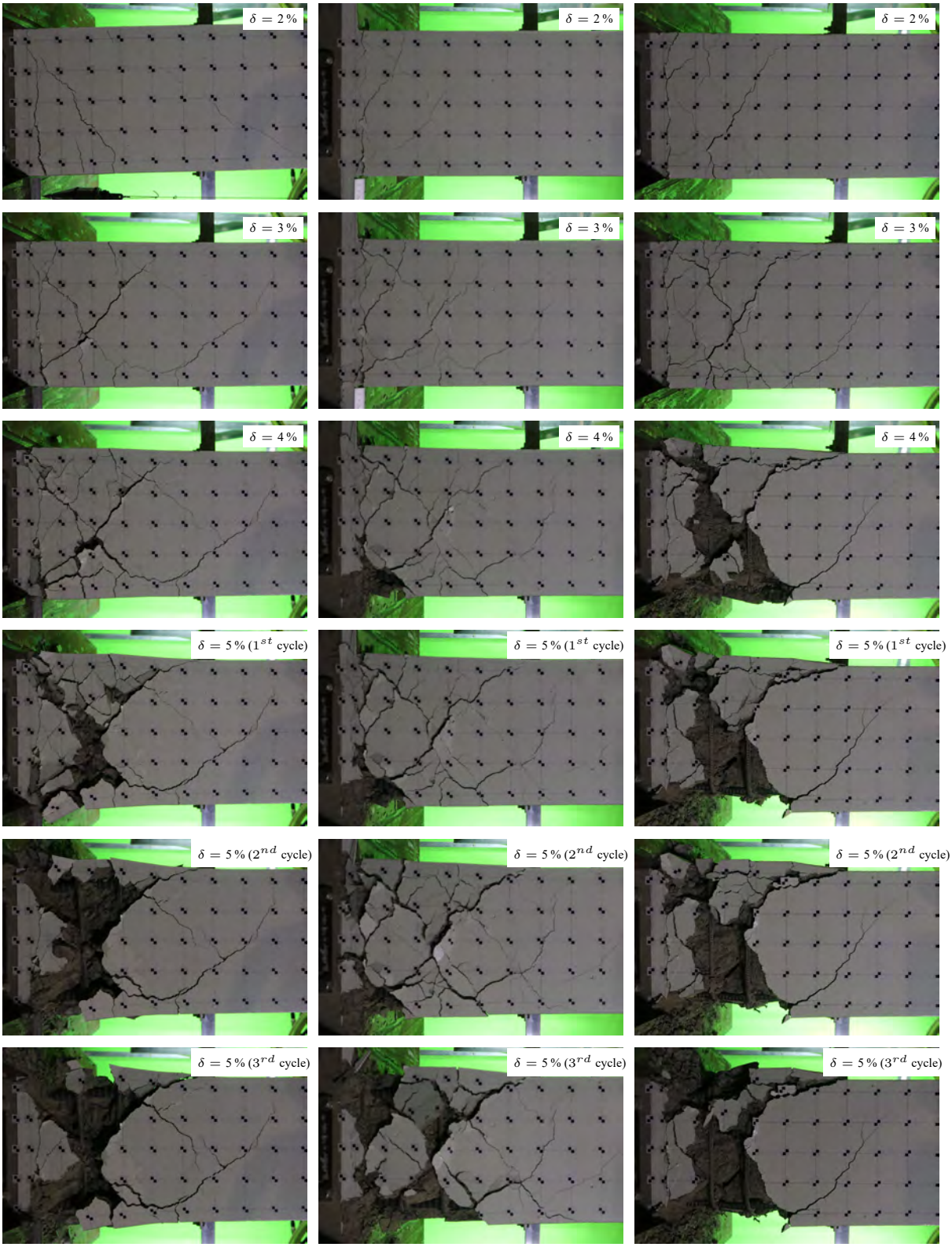

(a) SA-1 **(b) SA-2** **(c) SA-3**

Figure 6: Progress of damage at the critical section

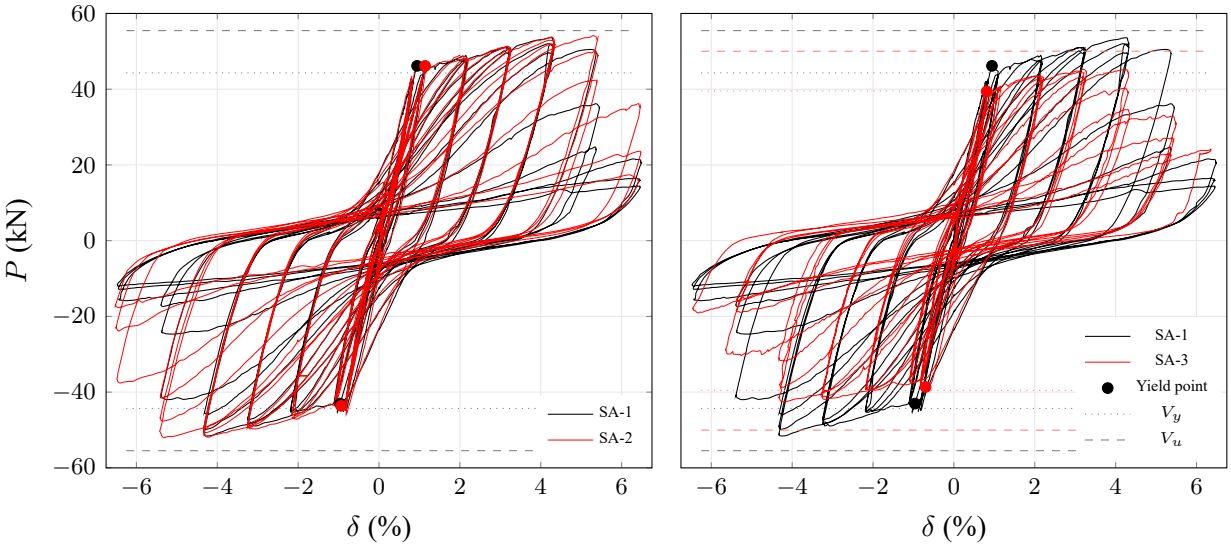

Figure 7: Drift vs lateral load relationship

horizontal grid 8. Large sways around a central were observed in the strains recorded at the exterior grids. However, strains recorded at the central grid were close to the mean. This can be easily explained from the theory of flexure which states that under pure bending top and bottom edges are subjected to equal compressive and tensile strains. Validity of the photogrammetric observations is further scrutinized by comparing the photogrammetric axial strain with the laser sensor recorded axial strain in Figure 9. Mean photogrammetric strain over the 5 vertical grids A to E is considered for comparison. Similar strain was obtained by the two measurement schemes for all the specimen up to the attainment of peak axial strain. Small variation observed after the peak strain may be attributed to the loosening of the laser target as the large cracks crept up to the point of fixture. Note that one of the laser sensors in SA-1 failed during operation and therefore no valid axial strain data could be recorded. Reported axial strain can also be related to the observation of loss of strength from force deformation relationship. Progressively accumulating axial strain was observed to peak at the 5 % drift cycle and drop in subsequent loading cycles due to crushing of the hinge concrete.

Lateral strains measured at the horizontal grids 3 to 8 of the hinge region are reported in Figure 10. Strains are calculated between the vertical grid point at A and E for each horizontal grid. Photogrammetric strain could not be measured at large deformations as the targets attached to the concrete surface fell off with the spalling concrete fragments. Gradually increasing strains were recorded at grids 8 and 7 throughout the experiment due to gradual penetration of cracks. At girds closer to the critical section, however, rapid expansion was observed during the 5 % drift cycle. Large strains exceeding 10 % were recorded during the 5 % drift loading cycle prior to the falling off of the photogrammetric target.

Comparison of the reported axial and lateral strains in specimens SA-1 and SA-3 is made in Figure 11. Axial strain was found peak at in the 4 % drift cycles in both the specimen but more rapid drop following the peak was observed in SA-3. Lateral strain at only grid-8 is considered for comparison. Lateral strain in SA-3 was observed to accumulate at a faster rate as compared to SA-1. However, no comparison could be made regarding peak strains as SA-3 lost the targets before reaching large strains. These observations clearly indicate greater deterioration of concrete and bulging of longitudinal reinforcement in the hinge region in SA-3.

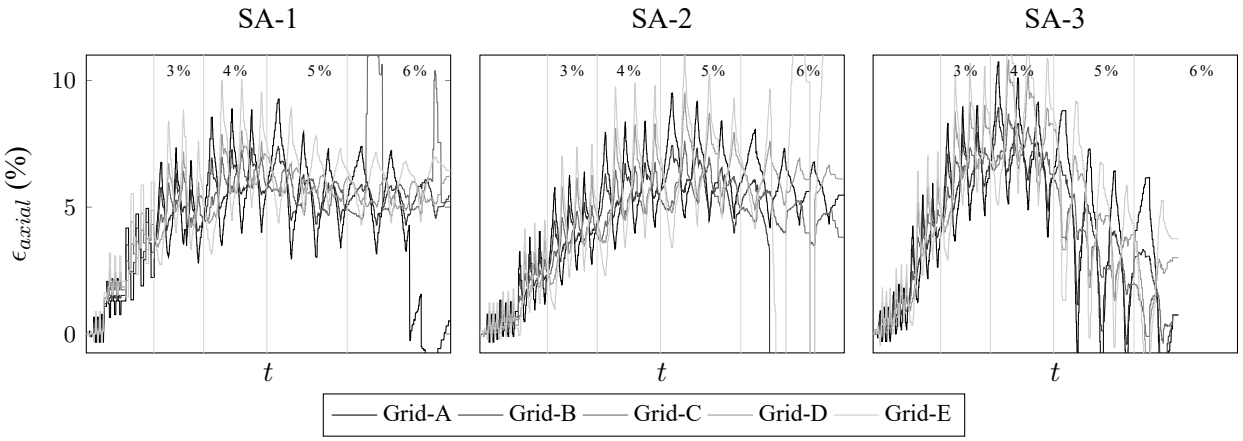

Figure 8: Photogrammetric measurement of axial strain at each grid

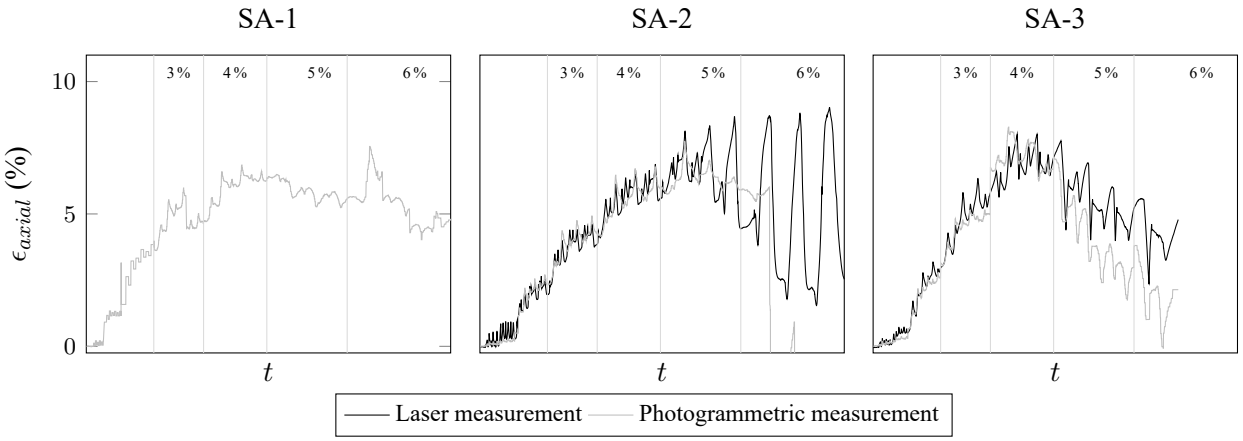

Figure 9: Comparison of photogrammetric and laser axial strain measurements

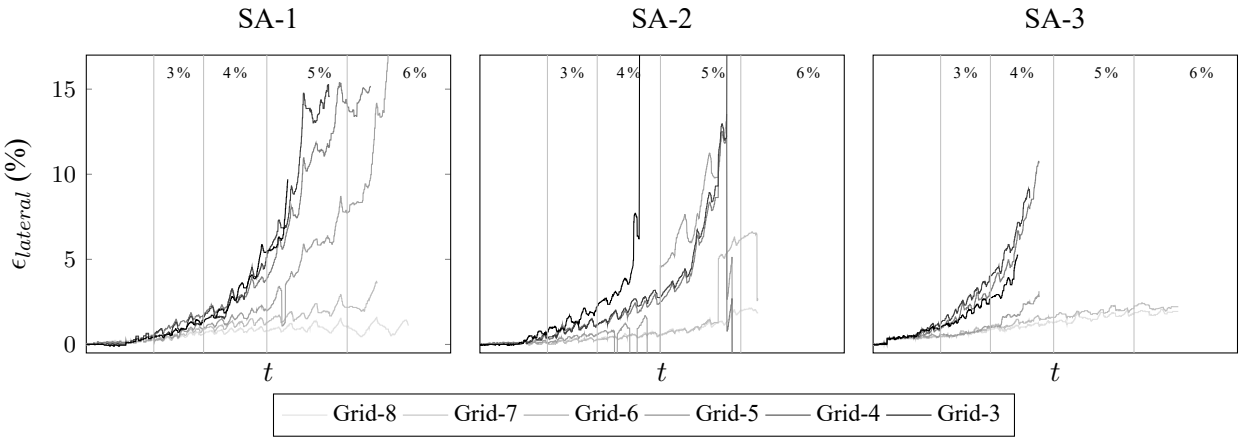

Figure 10: Photogrammetric measurement of lateral strain at individual grids

4. CONCLUSION

Influence of bar-buckling on the ultimate drift capacity of reinforced concrete beams was experimentally investigated. A simple stub-less specimen configuration was proposed and experimentally verified to reproduce cantilever response. In addition to the conventional measurements of tip displacement and

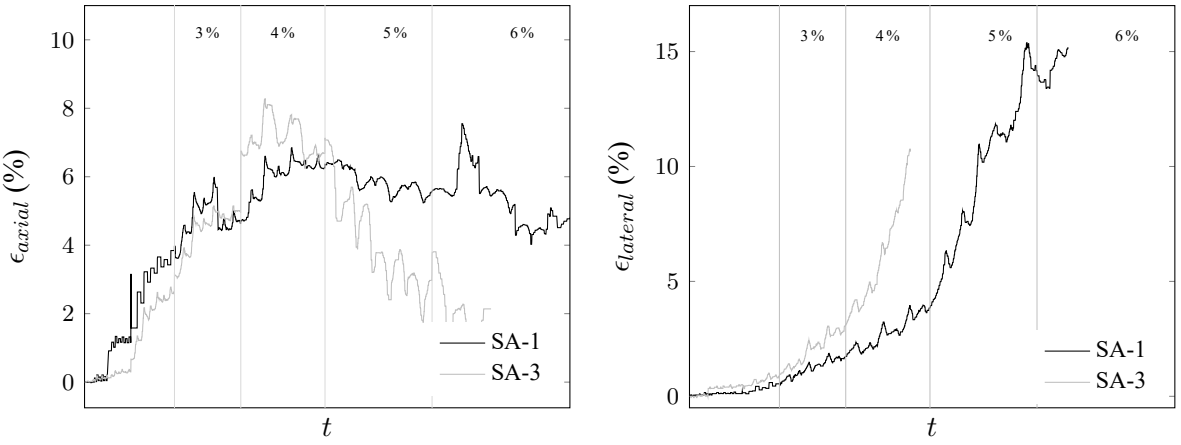

(a) Axial strain **(b) Lateral strain**

Figure 11: Comparison of strain development in specimen SA-1 and SA-3

hinge rotation, axial and lateral strains on the concrete surface were also recorded using an innovative photogrammetric measurement scheme. Findings from the comparative study of the response of two specimens reinforced with differing diameter longitudinal reinforcing bars can be summarized as follows:

- Ultimate drift capacity under reversed cyclic response was largely independent of the bar diameter.
- Overall cracking pattern starting from low drift levels to the ultimate state was also observed to be very similar in the two specimen.
- Greater deterioration of concrete in the hinge region starting at an earlier stage was observed in the specimen with smaller diameter bars.
- Axial and lateral strain recordings also identified comparatively greater disintegration of concrete, axial shortening and lateral bulging at the ultimate state in specimen with smaller diameter bars.

APPENDIX

Yield and ultimate strengths have been calculated as per ACI 318-14 [5] as follows:

Moment at yield (M_y) has been calculated using flexure theory under the assumptions of section 22.2 regarding concrete stress block parameters and maximum concrete compressive strain. Experimentally obtained material properties have been used in calculation. Ultimate moment strength (M_u) has been calculated as per the recommendations of section 18.6.1 regarding probable flexural strength. 1.25 times the yield reinforcement strength has been used to account for the effects of strain hardening.

Corresponding shear forces at yield and ultimate are then obtained as:

$$V_y = \frac{M_y}{L} \qquad \text{and} \qquad V_u = \frac{M_u}{L} \tag{1}$$

where L is the shear span.

ACKNOWLEDGMENTS

The authors wish to express their gratitude to the Grants-in-Aid for Scientific Research (KAKENHI) under Grant No. 16H04446 for the financial support of the research. The first author gratefully acknowledges the Japanese Government MEXT scholarship program.

REFERENCES

1) Charles F. Scribner and James K. Wight. Delaying Shear Strength Decay in Reinforced Concrete Flexural Members Under Large Load Reversals. Technical Report UMEE 78R2, The University of Michigan, 1978.
2) Matthew J. Moyer and Mervyn J. Kowalsky. Influence of tension strain on buckling of reinforcement in concrete columns. *ACI Structural Journal*, 100(1):75–85, 2003. doi: 10.14359/12441.
3) S. J. Pantazopoulou. Detailing for Reinforcement Stability in RC Members. *Journal of Structural Engineering*, 124(6):623–632, 1998. doi: 10.1061/(ASCE)0733-9445(1998)124:6(623).
4) Kenji Takita, Takafumi Aoki, Yoshifumi Sasaki, Tatsuo Higuchi, and Koji Kobayashi. High-Accuracy Subpixel Image Registration Based on Phase-Only Correlation. *IEICE transactions on fundamentals of electronics, communications and computer sciences*, 86(8):1925–1934, 2003. URL `http://ci.nii.ac.jp/naid/110003221273/en/`.
5) ACI Committee 318. Building Code Requirements for Structural Concrete and Commentary (ACI318-14). *American Concrete Institute*, Michigan, USA, 2014, 520p.